The role of visual angle in pattern phase transition of collective motions

Jiawei Li[1,3], Guanrong Chen[2] and Hai-Tao Zhang[1(a)]

[1] *School of Artificial Intelligence and Automation, the State Key Lab of Digital Manufacturing Equipment and Technology, and the Key Lab of Image Processing and Intelligent Control, Huazhong University of Science and Technology - Wuhan 430074, PRC*
[2] *Department of Electronic Engineering, City University of Hong Kong - Kowloon, Hong Kong*
[3] *China-EU Institite for Clean and Renewable Energy, Huazhong University of Science and Technology Wuhan 430074, PRC*

Abstract – Abundant collective motion patterns of animal groups have different kinds of functions like migration, predator avoidance and foraging. To explore the phase transition mechanism behind such charming collective behaviors, some self-propelled particle models have been proposed, most of which however have isotropic inter-particle interactions and hence could not reproduce sophisticated natural collective patterns. As a remedy, this letter develops an anisotropic self-propelled particle model. By slightly tweaking the vision range and inter-particle attraction, the proposed model demonstrate transitions between four distinct collective motion patterns, *i.e.*, torus, dumbbell, twist, and worm. To investigate more insightfully into the phase transition nature, quantitative analysis is carried out, revealing the relationship of visual angle-based inter-agent interactions and abundant pattern transitions existing in large numbers of natural, social and artificial grouping behaviors. From the industrial application point of view, the present study can help adjust the formation of multiple unmanned systems by simply tweaking a couple of vision-related parameters in their models.

Introduction. – A large variety of collective motions and behaviors in animal groups, such as fish schools [1–4], bird flocks [5–9], bacterium colonies and cell migrations [10,11] and human crowds [12,13], have been extensively studied. Recently, the fascinating patterns from such grouping behaviors have attracted more and more attention from scientists in biology, physics, system science, computer science, artificial intelligence and robotics. These motional pattern transitions can enable, for example, changing the collective motions of multiple unmanned vehicles, vessels or robots by simply tweaking a few parameters in their models [14].

In recent years, some dynamical models have been proposed to explore the inter-particle interactions contributing to coordinated motions of biological and engineering groups of dynamical systems. For instance, Olfati-Saber *et al.* proposed an inter-agent attraction/repulsion-based

dynamic model, which yields an α-lattice migration pattern with obstacle avoidance. Tanner *et al.* [15] showed that multi-agent systems (MASs) achieve velocity synchronization with stabilized patterns as long as the inter-agent communication graph always keeps jointly connected. Nagy *et al.* [16] extracted a hierarchical organization network behind the flight direction influential interactions among pigeon flocks. Zhang *et al.* [17] proposed an attraction-free MAS model, which guarantees asymptotic velocity synchronization in a bounded or periodically moving space.

Today, more and more efforts are devoted to studying the inter-agent interactive mechanisms leading to fascinating pattern transitions in both natural and artificial collective motions. Reynolds [18] introduced three fundamental rules, namely cohesion, separation, and alignment, for collective motions. Vicsek *et al.* [19] proposed a sensible inter-individual alignment model,

(a)E-mail: zht@mail.hust.edu.cn (corresponding author)

which reproduces a phase transition from a disordered state to an ordered state with decreasing external noise intensity or ascending particle density. Then, by equipping with inter-individual attraction and repulsion into the 2-dimensional Vicsek model [19], Couzin *et al.* [20] established a three-sphere model in a 3-dimensional space, which reproduces three typical collective motions, *i.e.*, swarming, flocking and torusing. Thereafter, several other Vicsek/Couzin-type models were developed to generate various motional patterns of self-propelled particle systems [21–24]. Recently, a quantitative assessment based on Vicsek model and the Toner and Tu theory is made by Mahault *et al.* [25], identifying the values of the associated scaling exponents differ significantly from those speculated in 1995. A new minimal MAS model was proposed by Vicsek *et al.* [26], merely based on inter-individual distances. In a comprehensive study on collective motional pattern transitions, Cheng *et al.* [27] analyzed phase transitions among four phases, *i.e.*, gas, crystal, liquid, and mill-liquid coexisting patterns, using a minimal model [28]. Furthermore, by varying the tendency of obstacle avoidance, they detected three distinct milling sub-phases, *i.e.*, ring, annulus, and disk. Trabesinger [14] pointed out that the work of Cheng et al. [27] helps capture various pattern phase transitions by tweaking the individual vision ranges of the particles and their tendency to avoid obstacles. More recently, Delgado *et al.* [29] revealed the role of within-group heterogeneity in the dynamics of animal collective motions. Singh *et al.* [30] proposed a boundary-driven dynamical self-propelled particles model where each one moves towards the farthest particle from itself. Thereby, an unusual pattern of assembly along lines is observed.

However, there still widely exist more sophisticated collective motional patterns that are not so regular like circles, ellipses and lattices. Such realistic patterns include "worms", "twist circles", "dumbbells" and their variants [26], which are often encountered in natural grouping and social gathering activities. To generate such irregular patterns, we propose an anisotropic minimal model with the assistance of a fixed distribution model [31]. The proposed model can generate pattern phase transitions among four interesting collective patterns, *i.e.*, twist, dumbbell, torus and worm, by slightly varying two interactive parameters.

Anisotropic minimal model. – Consider a group of N individuals moving in a 2-dimensional square $\Sigma = [0, L]^2$, $L > 0$ with periodic boundary conditions [19], described by

$$\dot{x}_i = v_0 \angle \theta_i,$$

$$\dot{\theta}_i = \frac{\gamma}{n_i} \sum_{i=1}^{n_i} \sin \lambda(\alpha_{ij} - \theta_i) + \sigma \mathrm{d}\xi, \tag{1}$$

where x_i, θ_i denote the position and moving direction of particle i, respectively; $\angle \alpha_{ij} = \angle \frac{x_j - x_i}{|x_j - x_i|}$; $\sigma \mathrm{d}\xi$ is the
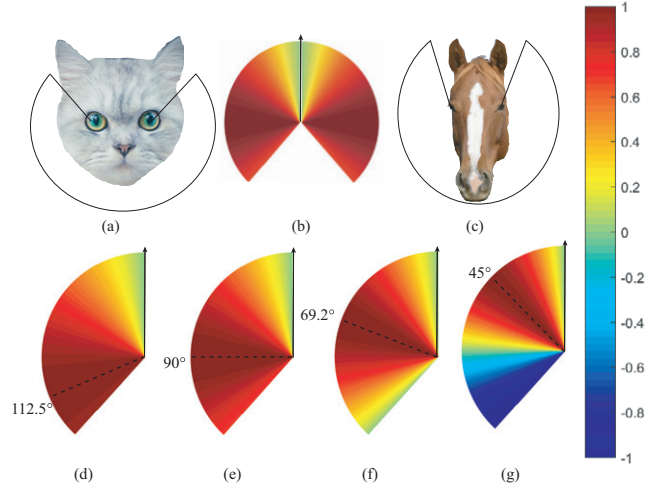

Fig. 1: Vision cones of typical carnivorous (cats (a)) and herbivorous (horses (c)) animals. Here, anisotropic attraction distribution with increasing λ is also exhibited, with color bar denoting the attraction strength. Subfigure (b) shows the distribution on both sides. For conciseness, it suffices to depict the left sides of the cones. (d) $\lambda = 0.8$; (e) $\lambda = 1.0$; (f) $\lambda = 1.3$; and (g) $\lambda = 2$. Interestingly, it can be observed that the attraction peak force appears at $\psi = 112.5°$ (rear), $90.0°$ (side), $69.2°$ (front) and $45.0°$ (front) for subfigures (d), (e), (f) and (g), respectively. This is consistent with the fact that attraction peaks at $\frac{\pi}{2\lambda}$.

external Gaussian white noise with amplitude σ; parameters γ, λ, v_0 and n_i are the interaction strength, attraction tuning parameter, unified particle speed, and number of neighbors in the vision cone of particle i, respectively. Here, λ is a parameter to tune the distribution of the inter-agent attraction force. The vision cone is defined by $|x_j - x_i| \leq R$ and $\angle \theta_i \cdot \angle \alpha_{ij} > \cos \beta$ with R and β denoting vision radius and angle range, respectively.

Apparently, the distribution of attraction in model (1) is not isotropic but follows the sine function. Note that the focal directions are distinct for different species of animals who have various attentions. As shown in fig. 1, the pupils of cats are located in front of their faces, which are often vertical to facilitate their focuses on upper and lower preys during ambushing. By contrast, large herbivores like horses, zebras and gnus generally live on flat grasslands. So, their pupils are located on both sides of their faces so as to focus their attention on herbaceous foods and neighbors beside.

In order to mimic the anisotropic influence of different attention patterns, we use a parameter λ in the present MAS model (1) to tune the amplitude along different directions. The distribution of the attraction directions in model (1) along increasing λ is shown in fig. 1. Therein, attraction peaks at $\frac{\pi}{2\lambda}$. Therefore, the influences of the front neighbors are intensified along increasing λ. The peak appears at $\psi = 112.5°$ (rear), $90.0°$ (side) and $64.3°$ (front) for subfigures (d), (e) and (f) of fig. 1, respectively.

However, when λ grows over $\frac{\pi}{\beta}$, the interactive force exerted by the rear neighbor(s) will switch from attraction to repulsion.

To quantitatively analyze the collective motion patterns, we now introduce two indices, *i.e.*, migratory order V_m and circular motion order V_c, as $V_m(t) = \frac{1}{N}|\sum_{i=1}^{N} v_i(t)|$ and $V_c(t) = \frac{1}{N}\sum_{i=1}^{N}|r_\eta(t) \times r_i(t)|$ with $r_i(t) = x_i - \overline{x}$, $\overline{x} = \frac{1}{N}\sum_{i=1}^{N} x_i(t)$, $v_i(t) = v_0 \angle \theta_i(t)$, and "×" denoting cross product. Clearly, the more directionally synchronized the system is, the larger the value V_m is, until it reaches the maximum value 1. Analogously, the more circular the system's motion is, the larger the value V_c is, until it reaches the maximum value 1, representing a standard circular motion. Besides, in order to quantify the collective patterns more precisely, we propose an average dynamical curvature index $\overline{\eta}(t)$, as $\overline{\eta}(t) = \frac{1}{N}\sum_{i=1}^{N}\eta_i(t)$ and $\eta_i(t) = \frac{2\sin\phi_i}{|x_i(t+1)-x_i(t-1)|}$, with $\phi_i = \arccos\frac{(x_i(t+1)-x_i(t))(x_i(t-1)-x_i(t))}{|x_i(t+1)-x_i(t)|\cdot|x_i(t-1)x_i(t)|}$ quantifying the curvature of the arc formed by the three picked consecutive snapshots along the moving trajectory of the particle i. Significantly, $\overline{\eta}(t)$ quantifies the tendency to change the group moving directions.

Numerical simulations and analysis. – Now, we conduct numerical simulations, where the initial moving directions of the N particles are randomly picked from $[0, 2\pi]$. The parameters in model (1) are set to $N = 100$, $L = 4$, $v_0 = 1$, $R = 1$, $\gamma = 5$, and $\sigma = 0$, as in [31]. A sufficiently large density $\rho = N/L^2$ is imposed to ensure that the particles of the group are all connected. By slightly tuning the attraction distribution parameter λ and the view angle threshold β, as shown in fig. 2, the emergence of four distinct phases are observed, *i.e.*, i) *Torus*: bidirectional milling phase, where half of the particles rotate anticlockwise while the other half clockwise. ii) *Dumbbell*: an "8"-shaped rotating chain with one intersection at the center moving straightly forward (as indicated by the arrows). iii) *Twist*: a rotating chain with two intersections. iv) *Worm*: particles creep along a curved line like a worm [31] (slight noise is induced in formation). Evidently, torus corresponds to $V_c \simeq 1$ and $V_m \simeq 0$, whereas worm to $V_c \simeq 0$ and $V_m \simeq 1$. As an intermediate phase, twist shows a medium level of circular motion around $V_c = 0.4$ without migration motion, $V_m = 0$. By contrast, dumbbell with a moving group center and two rotating circular chains corresponds to $V_c \in (0.61, 0.67)$ and $V_m \in (0.35, 0.41)$. Torus corresponds to a high curvature $\overline{\eta}$, which grows higher with increasing λ. Dumbbell has a greater $\overline{\eta}$ than twist, and $\overline{\eta}$ of both patterns drops with increasing λ.

To illustrate the influence of the attraction distribution parameter λ, we fix $\beta = 2.4$ and show the occurrence probability of the four patterns with increasing λ. We observe torus and worm when λ is less than 0.87 or greater than 1.2, respectively. Meanwhile, the intermediate rotating chains and dumbbell phases and their coexistence
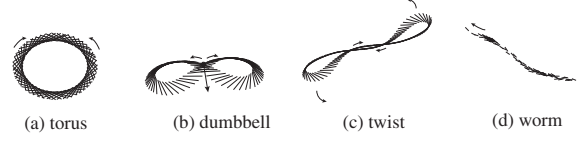

Fig. 2: Four stable collective motional patterns generated by the proposed minimal model (1).
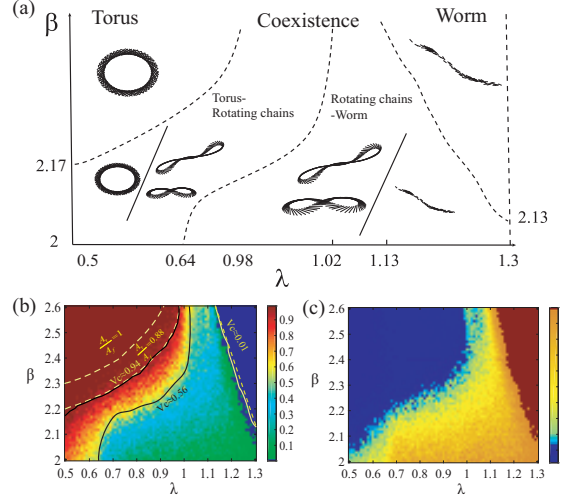

Fig. 3: (a) Phase transition sketch map. (b), (c): heat map of circular motion parameter V_c (b) and migration motion parameter V_m (c) *vs.* attraction force parameter λ and view angle β. Contour lines in (b) determine the boundaries of different phases. The top-right dotted line shows the analytical boundary between worm phase and rotating chains-worm coexisting phase according to eq. (2), and the top-left dotted line exhibits the analytical boundary between torus phase and rotating chains-torus coexisting phase according to $\frac{A_r}{A_f} = 1$. Parameters: $N = 100$, $L = 4$. Each point is an average over 50 independent runs.

emerge for $\lambda \in [0.87, 1.2]$. A plausible explanation of the phase transition is that the polarization effect is intensified with increasing λ, and hence the corresponding phase pattern is elongated from torus to dumbbell/twist, and then to worm. More precisely, as λ increases over 0.87, the centripetal force descends due to the decreased attraction or increased repulsion, so some torus patterns transform into twists/dumbbells. As λ grows further, all rotating phases become unstable, an unidirectional rotating arc is observed as a critical state. Thereafter, when λ surpasses 1.2, the rotational effect disappears, corresponding to worm. Meanwhile, it is found that cumulative agents distribute on one side of the dumbbell/twist pattern when λ grows larger. Thus, more attraction is yielded by the front neighbors, so particles are more likely to move on one particular track rather than spread over the whole formation.

To show the pattern phase transition more vividly, we exhibit the entire β-λ phase diagram in fig. 3(a) for the self-propelled particles described by model (1). It
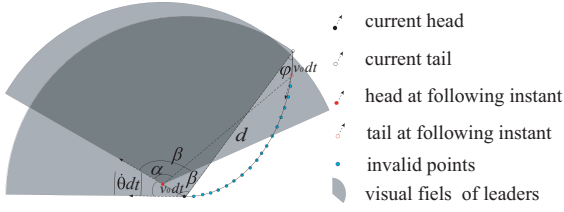
Fig. 4: Geometrical explanation of polarized patterns. Here, β, d, d', ϕ are the view angle, distance between the current head and tail, distance between the next head and tail, and initial angle of the tail relative to the head, respectively. Angle α, between the next heading of the leader and a vector pointing from the leader to the tail at the next time, represents the angle required to detect the group tail.

Fig. 5: Evolution of angle required to detect group tail α (a) and the proportion of rear attraction to front attraction $\frac{A_r}{A_f}$ (b) with increasing attraction tuning parameter λ for different view angle β.

can be observed that the torus, torus/twist/dumbbell, worm/twist/dumbbell, and worm phases appear in the top-left, middle top-left, middle bottom-right and top-right blocks of the β-λ space in fig. 3(a), respectively. The phase map shows that the tendency of the polarized motion is intensified with increasing λ. Meanwhile, the centripetal force increases with ascending view angle β in low λ scenario. Once λ increases beyond a threshold ($\lambda_c = 1.13$), the increase of β will lead to a polarized pattern like a worm (the top-right block of the β-λ space in fig. 3(a)). To quantify the phase transition, we present a heat map in the V_c (respectively, V_m) space in fig. 3(b) (respectively, fig. 3(c)), which exhibits the tendency of circular (respectively, polarized) motion with β and λ. The contours depicted in the V_c heat map suggest that large ($\beta > 2.5$) or small ($\beta < 2.1$) view angles have little influence on the phase transition due to the fringe effect. The descending tendency of V_c shown in fig. 3(b) corresponds to the ascending trend of V_m in fig. 3(c), as a consequence of the extreme opposite motion patterns exhibited by torus ($V_m \simeq 0$, $V_c \simeq 1$) and worm ($V_m \simeq 1$, $V_c \simeq 0$). Distinctively, the boundaries of the four phases surface can be used to predict the phases.

To investigate the phase transition mechanism more carefully, we conduct a qualitative analysis. Indeed, a rotational pattern emerges when the group head turns sufficiently sharply to meet its tail [32]. To reveal the forming criterion for the rotational patterns, *i.e.*, torus, dumbbell and twist, we quantitatively find the critical state, where the transition occurs as shown in fig. 4. As can be seen, when the tail of a group enters the vision cone of its head, the head will begin to deflect around due to the centripetal attraction by the group tail. The angle of this deflection, α, determines whether the group will transform into rotating patterns or remain a worm. More precisely, given a fixed velocity v_0, initial angle ϕ and head-to-tail distance d, the parameter α shrinks with increasing the defection angle $|\dot{\theta}|\mathrm{d}t$. When α descends to be less than the view angle β, implying that the head still captures its tail, the transition changes from worm to torus. Otherwise, the group tail will be lost to
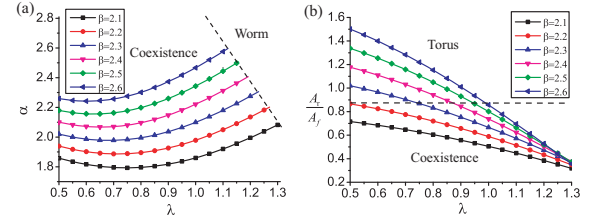
its head, therefore such transition will not happen. To give a geometrical explanation, we assume that the curvature of the pattern depicted in fig. 4 is constant, and hence it can be regarded as an arc. Thereby, one has $\sin(\phi + \alpha + |\dot{\theta}|\mathrm{d}t - \beta)v_0\mathrm{d}t = \sin(\alpha + |\dot{\theta}|\mathrm{d}t - \beta)\mathrm{d} - \sin\alpha v_0\mathrm{d}t$ and $\phi = \pi - \beta$, which immediately leads to

$$\sin(2\beta - \alpha - \gamma\sin(\lambda\beta)\mathrm{d}t)v_0\mathrm{d}t =$$
$$\sin(\alpha + \gamma\sin(\lambda\beta)\mathrm{d}t - \beta)\mathrm{d} - \sin\alpha v_0\mathrm{d}t, \qquad (2)$$

with the turning rate $|\dot{\theta}| = \gamma\sin(\lambda\beta)$ as shown in fig. 4.

Recall that $\alpha < \beta$ ensures the group head to turn a sufficiently large angle to capture its tail. Hence, as can be seen, with the same $|\dot{\theta}|$, the index α descends as the head-tail distance d increases. Thus, $d = R$ determines the lower bound of α. In such a situation, only worm is formed when $\alpha > \beta$, otherwise rotating patterns appear. Thus, it has been verified that a larger α indicates an enhanced tendency of transition from a rotating pattern to a polarized one like the worm.

Now, we solve eq. (2) with parameters $\gamma = 5$, $d = R = 1$, $v = 1$ and $\mathrm{d}t = 0.1$, so as to quantify the correlation between α and λ. For $\lambda \in [0.5, 1.3]$, the numerical solution is exhibited in fig. 5. Minimal value appears at $\frac{\pi}{2\beta}$, where attraction peaks at the edge of the vision cone. Then, the index α monotonously increases with increasing λ. Once λ grows over a threshold (*e.g.*, $\lambda = 1.13$ for $\beta = 2.6$, as depicted in fig. 5(a)), where the required detection angle α is equivalent to the view angle β, all rotating patterns cannot be maintained because the deflection is not large enough.

Next, we increase β to be in the range of $[2, 2.6]$. Together with $\alpha < \beta$, the result predicts the boundary of rotating patterns as well as worm coexisting phase and the worm phase, as the dotted lines shown in the top-right part of fig. 3(b). This quantitatively verifies that the boundary in fig. 3(b) matches the observation of the phase transition in fig. 3(a) quite well. In addition, close to the boundary where $\alpha \simeq \beta$, the head-tail distance of the worm in fig. 4 is stationary, which well explains the emergence of the rotating arcs.

Now, we illustrate the polarized pattern of the critical state shown in fig. 4, with sufficient attraction yielded by front neighbors. Once such a critical state is formed, bidirectional milling torus can no longer emerge, because the group leader will only detect its tail from one side. So, for

the emergence of torus phase, more attraction from the rear is required for the particle with symmetrical vision to turn around from either side.

Next, we calculate the proportion of rear attraction to front attraction, as $\frac{A_r}{A_f} = \frac{\int_{\frac{\pi}{2}}^{\beta} \sin(\lambda\theta_{def})\mathrm{d}\theta_{def}}{\int_0^{\frac{\pi}{2}} \sin(\lambda\theta_{def})\mathrm{d}\theta_{def}}$, where A_r and A_f denote the attractions from front and rear, respectively, and θ_{def} is the deflection angle from the moving direction. The angle of A_r is defined as $\theta_{def} \in [\frac{\pi}{2}, \beta]$ and A_f as $\theta_{def} \in [0, \frac{\pi}{2}]$.

The numerical solutions with different β are exhibited in fig. 5(b). The boundary between torus and other rotating patterns can be calculated, assuming $\frac{A_r}{A_f} = 1$. The corresponding results are shown as dotted lines in the top-left part of fig. 3(b). We differentiate torus phases from rotating chains by $V_c \approx 0.94$ in the heat map as shown by fig. 3(b) with solid lines, as few rotating chains appear for $V_c > 0.94$. Significantly, the boundary identified by $V_c \approx 0.94$ nicely fits the value of $\frac{A_r}{A_f} = 0.88$, as shown in fig. 5(b) and fig. 3(b). Furthermore, more elongated group patterns, such as twist and dumbbell, emerge from the increasing tendency of the polar motion caused by increasing λ or reducing β. Specifically, dumbbell is formed when the transformation state in fig. 4 is lengthened beyond the detection zone of the group head, hence the head captures the middle part of the group instead of the tail. The analytical result is thus verified.

Conclusions. – In this letter, we have proposed a minimal attraction model with adjustable vision distribution to mimic the distinct focusing motional directions of different animals in nature. Four distinguishing dynamical patterns, *i.e.*, torus, dumbbell, twist and worm, are observed by tweaking two parameters: attraction parameter λ and view angle β. Quantitative analysis is presented to explain the phase transition mechanism, which can be used to predict the final patterns. Our results shed some lights onto the mechanism of multiple flocking formation observed in nature, such as rotational patterns in fish schools [33] and the transition from file formation to encircling motion found in sheep herds and ant colonies [33,34].

Our study is expected to provide a new perspective for better understanding the emergence of various self-organized biological and social collective motions arising from inter-particle interactions. The phase transition triggered by tuning a couple of system parameters may have potential applications in formation control and coordination of industrial and engineering multi-agent systems, like unmanned vehicle systems, unmanned water surface vessels, and sensor networks.

$$* * *$$

REFERENCES

[1] Shaw E., *Am. Sci.*, **66** (1978) 166.
[2] Becco C., Vandewalle N., Delcourt J. and Poncin P., *Physica A*, **367** (2006) 487.
[3] Makris N. C., Ratilal P., Symonds D. T., Jagannathan S., Lee S. and Nero R. W., *Science*, **311** (2006) 660.
[4] Kadri U., Brümmer F. and Kadri A., *EPL*, **116** (2016) 34002.
[5] Hayakawa Y., *EPL*, **89** (2010) 48004.
[6] Cavagna A., Cimarelli A., Giardina I., Parisi G., Santagati R., Stefanini F. and Viale M., *Proc. Natl. Acad. Sci. U.S.A.*, **107** (2010) 11865.
[7] Ballerini M., Cabibbo N., Candelier R., Cavagna A., Cisbani E., Giardina I., Lecomte V., Orlandi A., Parisi G., Procaccini A., Viale M. and Zdravkovic V., *Proc. Natl. Acad. Sci. U.S.A.*, **105** (2008) 1232.
[8] Chen D., Vicsek T., Liu X., Zhou T. and Zhang H. T., *EPL*, **114** (2016) 60008.
[9] Flack A., Nagy M., Fiedler W., Couzin I. D. and Wikelski M., *Science*, **360** (2018) 911.
[10] Estudillo Y. A., Krieg M., Stühmer J., Licata N. A., Muller D. J. and Heisenberg C.-P., *Curr. Biol.*, **20** (2010) 161.
[11] Zhang H. P., Be'er A., Smith R. S., Florin E.-L. and Swinney H. L., *EPL*, **87** (2009) 48011.
[12] Helbing D., Farkas I. and Vicsek T., *Nature*, **407** (2000) 487.
[13] Barbosa H., Barthelemy M., Ghoshal G., James C. R., Lenormand M., Louail T., Menezes R., Ramasco J. J., Simini F. and Tomasini M., *Phys. Rep.*, **734** (2018) 1.
[14] Trabesinger A. H., *Nat. Phys.*, **18** (2016) 103005.
[15] Garnier S., Gautrais J. and Theraulaz G., *Swarm Intell.*, **1** (2007) 3.
[16] Nagy M., Ákos Z., Biro D. and Vicsek T., *Nature*, **464** (2010) 890.
[17] Zhang H.-T., Zhai C. and Chen Z., *IEEE Trans. Autom. Control*, **56** (2011) 430.
[18] Reynolds C. W., *SIGGRAPH Comput. Graph.*, **21** (1987) 25.
[19] Vicsek T., Czirók A., Ben-Jacob E., Cohen I. and Shochet O., *Phys. Rev. Lett.*, **75** (1995) 1226.
[20] Couzin I. D., Krause J., James R., Ruxton G. D. and Franks N. R., *J. Theor. Biol.*, **218** (2002) 1.
[21] Jadbabaie A., Lin J. and Morse A. S., *IEEE Trans. Autom. Control*, **48** (2003) 988.
[22] Baglietto G. and Albano E. V., *Phys. Rev. E*, **78** (2008) 021125.
[23] Ginelli F., Peruani F., Bär M. and Chaté H., *Phys. Rev. Lett.*, **104** (2010) 184502.
[24] Costanzo A., *EPL*, **125** (2019) 20008.
[25] Mahault B., Ginelli F. and Chaté H., *Phys. Rev. Lett.*, **123** (2019) 218001.
[26] Vicsek T. and Zafeiris A., *Phys. Rep.*, **517** (2010) 71.

[27] Cheng Z., Chen Z., Vicsek T., Chen D. and Zhang H.-T., *New J. Phys.*, **18** (2016) 103005.

[28] Shimoyama N., Sugawara K., Mizuguchi T., Hayakawa Y. and Sano M., *Phys. Rev. Lett.*, **76** (1996) 3870.

[29] Delgado M. d. M., Miranda M., Alvarez S. J., Gurarie E., Fagan W. F., Penteriani V., Virgilio A. d. and Morales J. M., *Philos. Trans. R. Soc. B*, **373** (2018) 20170008.

[30] Singh K. and Rabin Y., *Sci. Rep.*, **9** (2019) 17910.

[31] Barberis L. and Peruani F., *Phys. Rev. Lett.*, **117** (2016) 248007.

[32] Strömbom D., *J. Theor. Biol.*, **283** (2011) 145.

[33] Parrish J. K., Viscido S. V. and Grünbaum D., *Biol. Bull.*, **202** (2002) 296.

[34] Toulet S., Gautrais J., Bon R. and Peruani F., *PLoS ONE*, **10** (2015) 1.